Pergamon

Scripta Materialia, Vol. 38, No. 2, pp. 215–221, 1998
Elsevier Science Ltd

1359-6462/98 $19.00 + .00

PII S1359-6462(97)00472-7

THE STUDY ON MICROSTRUCTURAL AND MECHANICAL PROPERTIES OF WELD HEAT AFFECTED ZONE OF 7075-T651 ALUMINUM ALLOY

R.Y. Hwang and C.P. Chou
Department of Mechanical Engineering, National Chiao Tung University,
Hsinchu, Taiwan, R. O. C.

(Received May 5, 1997)
(Accepted August 5, 1997)

Introduction

Aluminum alloys play an important role in aerospace industry due to their high strength and low density. The general accepted precipitation behavior of 7075 alloy was represented as: supersaturated solid solution $\alpha_{ss} \rightarrow$ GP zones $\rightarrow \eta'(MgZn_2) \rightarrow \eta(MgZn_2)$. The Addition of Cu in Al-Zn-Mg alloy would promote the transformation of GP zones into $\eta'(MgZn_2)$ phase and stabilize the $\eta(MgZn_2)$ phase [1]. The T6 temper has the maximum strength but lower ductility. The T73 temper may lose some strength, but can gain higher corrosion resistance and lower susceptibility to stress corrosion cracking as compared to the T6 temper.

The welding fabrication can produce thermal cycling on the weldment. In heat affected zone (HAZ) besided to the fusion zone, different temperatures can be obtained. This would cause change of microstructure in the HAZ of aluminum alloy weldment. Many workers [2–5]studied on behavior of weld HAZ by cutting the HAZ into many small pieces or using short time isothermal heat treatment to simulate the HAZ. This may lose some information, specially near the fusion zone, because high temperature gradient occurred in this region. In this study, the Gleeble system was used to simulate the weld HAZ. It can accurately simulate every point of weld HAZ by heating and cooling the specimen to the thermal history of weld HAZ as the same as measured. The microstructural and mechanical properties of weld HAZ of 7075-T651 alloy was investigated.

Experimental Procedures

Commercial 7075-T651 aluminum alloy of 3 mm thickness was used in this study. The chemical composition was shown in Table 1. Gas tungsten-arc welding (GTAW) was performed using AC current. The heat input was 610 J/mm for a single-pass full penetration weld on the 3 mm aluminum alloy sheet. The measured thermal cycles are shown in Fig. 1. These five HAZ thermal cycles were individually simulated to specimens by Gleeble 1500 simulator. The specimens were machined to the dimension of 130 mm × 15 mm × 3 mm and heated to the same thermal history as those measured. The temperature error was controlled below 5 °C. For convenient identification of the simulated specimens, the thermally cycled specimens were to be referred to the peak temperature of thermal cycle.

TABLE 1
Chemical Composition of 7075 Alloy

Cu	Zn	Mg	Fe	Si	Mn	Cr	Ti	Al
1.70	6.08	2.54	0.26	0.10	0.03	0.20	0.05	bal

For example, the A546 specimen was referred to the 546 °C peak temperature of thermal cycle. The base metal was referred as BM.

Calorimetric measurements were made using a Perkin-Elmer DSC7 Thermal Analyzer. Sample disc about 60 mg was prepared from each of the five simulated HAZ specimens. To increase the sensitivity of the measurements, a high purity aluminum disc was used as a reference. Several runs were made at a heating rate of 10 °C/min over the range from room temperature to 520 °C. Dried nitrogen of flow rate 40 ml/min was passed through the calorimeter to minimize oxidation. In order to compare the relative heat capacity of samples, the measured data were transformed proportionally to heat capacity of 100 mg. Subsequently, a linear baseline was subtracted from the data. This baseline represents the temperature dependent heat capacity of aluminum-rich solid solution and existing precipitates [6,7].

Vickers hardness test was used (at a 50 kg load) to determine the difference of hardness for each temper of weld HAZ. The stress-strain behavior of each temper was measured using tensile test. The fractured specimens of tensile tests were examined by SEM. Specimens for transition electron microscopy (TEM) were made by conventional methods of jet electropolishing, using a solution of 33% nitric acid in methanol at −15 °C. TEM was examined by the JEM 4000 FX microscope.

Results and Discussion

Thermograms characteristic of each temper of simulated weld HAZ have noticeable difference, as shown in Fig. 2 and Fig. 3. There are four endothermic peak; peak I (130), peak II (190), peak III (230–240 °C) and peak IV (430 °C). Besides, two exothermic peak (peak V and peak VI) were also observed. The peak I represents the dissolution of GP zones [8,9]. It referred that specimen contained GP zones, which were dissolved during DSC scans. The peak II represents the dissolution of η' phase [9–14]. The peak III represents dissolution of η' phase and small η phase [11,15]. The peak IV represents the dissolution of η phase that is existed before DSC scans or produced during DSC scans.

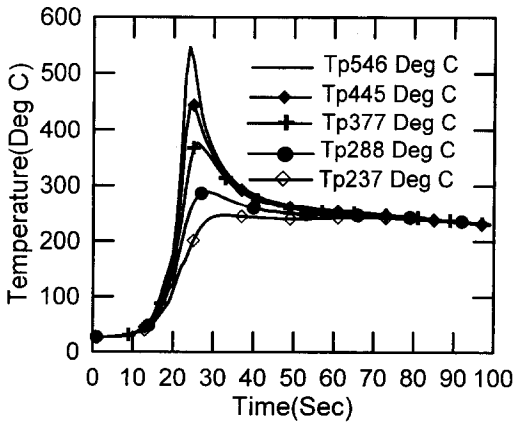

Figure 1. The measured thermal cycles of weld HAZ.

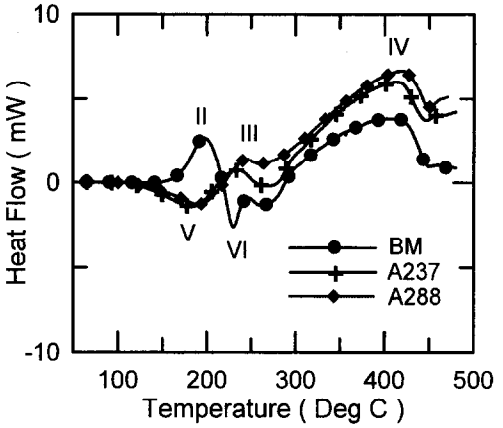

Figure 2. Thermograms of the base metal, A237 and A288.

The thermograms of the base metal, the A237, and the A288 are shown in Fig. 2. The T651 base metal was a reasonable schematic representation of the results of numerous observations [9–14]. The appearance of peak II at peak temperature 190 °C was due to the dissolution of η' phase, which is the main precipitate of T651 temper confirmed by TEM investigation [9,12,13]. The exothermic peak VI and the endothermic peak IV were produced primarily during DSC scan. The thermogram of The A237 shows exothermic peak V and endothermic peaks III and IV. Peak V was caused by η' phase re-precipitation during the subsequent DSC scan. This temper sustained 237 °C peak temperature of thermal cycle. Some of small η' phase was dissolved after thermal cycling and reformed again during DSC scan [16]. The peak III was caused by the dissolution of coarsening η' phase and small η phase. The peak IV was caused by the dissolution of η phase, which was existed after thermal cycling or created by DSC scan. The A237 temper may contain some of dissolution of η' phase, survived η' phase and small amount of η phase. The thermogram of the A288 is similar to that of the A237 except more pronounced peak III are observed. That referred to more η phase would be existed after welding.

The thermograms of the A377, the A445 and the A546 are shown in Fig. 3. The A377 had small peak VI and large peak IV. The exothermic peak VI was opposite in sign to the peak III. This indicated that

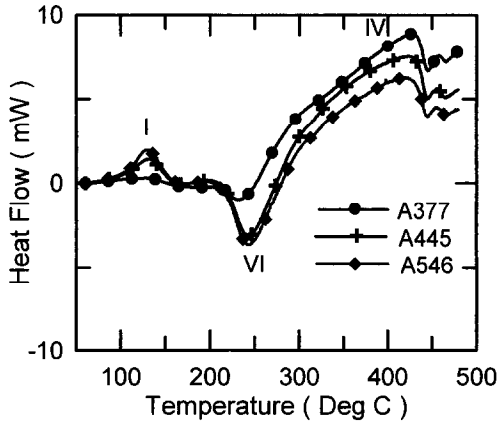

Figure 3. Thermograms of the A377, A445 and A546.

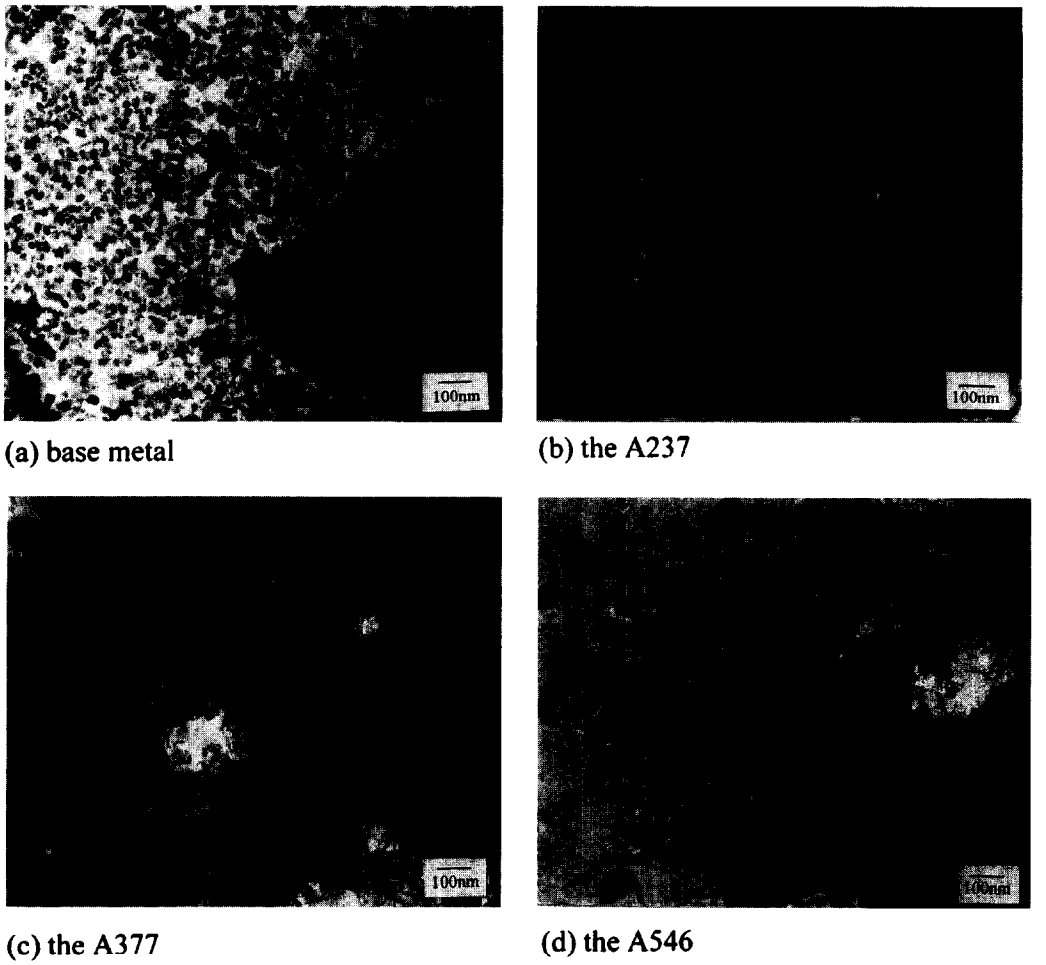

(a) base metal (b) the A237

(c) the A377 (d) the A546

Figure 4. The TEM microstructure of simulated weld HAZ.

some of coarsening η' phase and small amount of η phase may be dissolved after thermal cycling and precipitated again during DSC scan. Peak IV would be contributed by DSC scan, but most of that were contributed by the precipitation of η phase after thermal cycle was performed. The A377 contained large amounts of η phase and a small amount of supersaturated solid solution. The A445 and The A546 had peak I, peak VI and peak IV. Peak I was caused by the dissolution of GP zones which were formed after thermal cycling. Exothermic peak VI was caused by partial dissolution of η phase after thermal cycling and then reprecipitation during DSC scan. The two tempers contained primarily GP zones and η phases as expected.

The TEM micrographs are consistent with the results of DSC scan. Fig. 4 shows the TEM bright field image of each temper of simulated HAZ. Large amounts of η' phase in matrix were observed on T651 temper as shown in Fig 4(a). The A237 displayed the coarsening η' and η phase precipitates and small amount of precipitate as shown in Fig. 4(b). The A377 displayed the large amount of coarsening η phase precipitates as shown in Fig. 4(c). The A546 displayed the coarsening and small amount of η phase as shown in Fig. 4(d). The amount of coarsing η phase was small than that of the A377 temper because partial η phase was dissolved during welding.

TABLE 2
The Mechanical Properties of Simulated Weld HAZ

Temper	Yield Strength (MPa)	Ultimate tensile Strength (MPa)	Elongation (%)	Hardness (Hv)
T6	512	584	12.7	180
A237	460	529	13.9	163
A288	398	481	14.6	145
A377	249	386	20.8	107
A445	341	502	20.5	135
A546	322	478	15.9	133

Table 2 shows the tensile test results of each temper of simulated weld HAZ. The major strengthening phase of 7075 alloy was η' phase. The T651 temper has the maximum amount of precipitate of η' phase and therefore has the maximum strength but with the lowest ductility. Both hardness and strength of the A237 are lower than that of the base metal. This was due to small η' phase dissolution and some of η' phase growth after thermal cycling. The hardness and strength of the A288 were lower than that of the A237, because more η' phase was dissolved and more η phase was formed during thermal cycling. The minimum strength and the maximum ductility can be obtained at the A377. This was caused by large amount of precipitation of η phase. The A445 and the A546 were partial solution treatments. The reprecipitation of GP zones after thermal cycling would provide strengthening effect. This can cause strength recovery even the peak temperature sustained were higher than the A377 temper.

Figure 5 shows the relationship between yield strength, elongation, and peak temperature of simulated weld HAZ. Between peak temperature 237 °C and 377 °C, the strength decay was caused by the dissolution of η' phase and transformation to the η phase. Between peak temperature 377 °C and 546 °C, the strength recovery was caused by the dissolution of η phase and the transformation to the GP zones. The strength decay of weld HAZ was caused by the formation and coarsening of η phase. The result of elongation was opposite to that of the yield strength due to the precipitation of GP zones and η' phase, and was related to the precipitation of η phase in weld HAZ.

Figure 6 shows the SEM fractograph of several tempers of simulated weld HAZ. The T651 base metal showed the semi-brittle appearance as shown in Fig. 6(a). The ductile dimples fracture were observed in the A237 and the A377 as shown in Fig. 6(b) and 6(c) respectively. The A377 contained

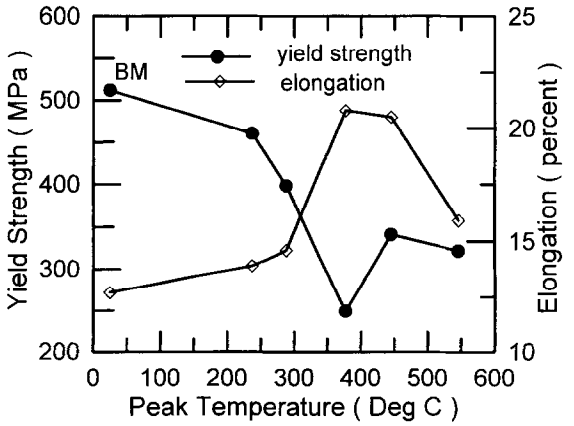

Figure 5. Yield strength and elongation of simulated HAZ.

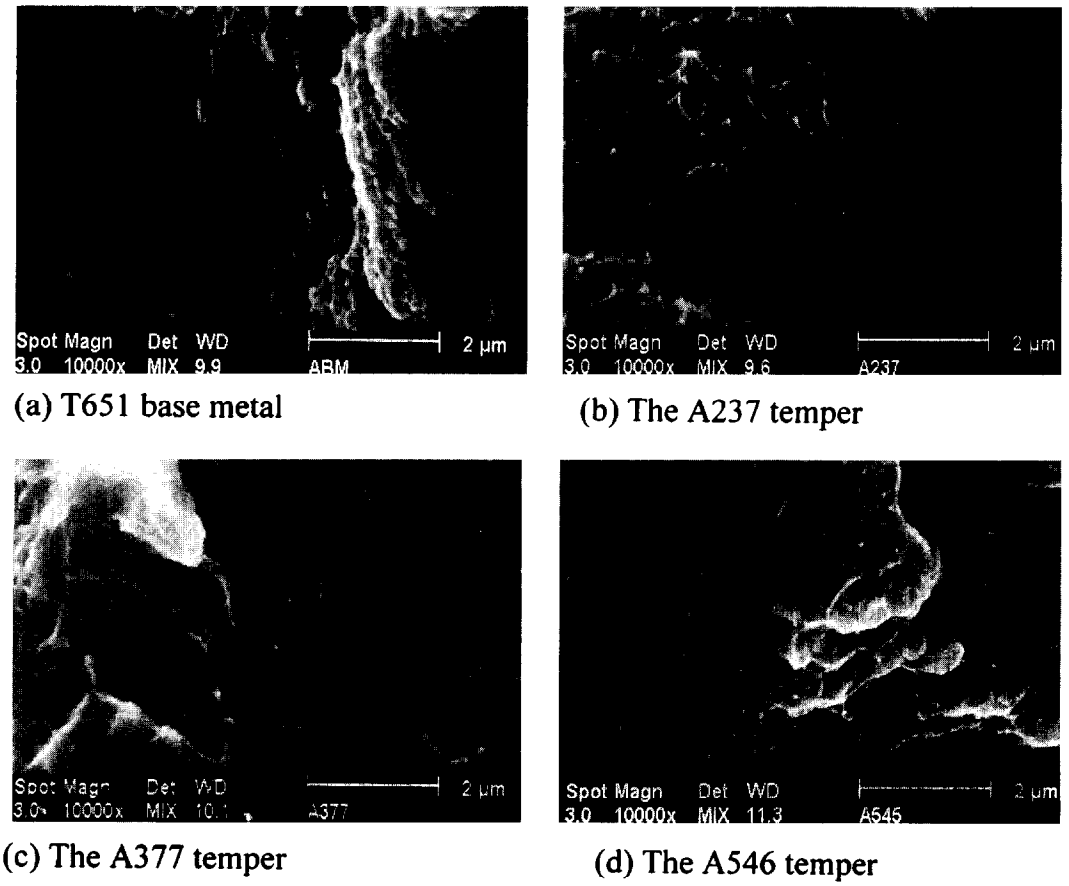

Figure 6. The SEM fractographs of base metal and simulated weld HAZ.

the maximum amount of η phase and have the maximum dimple appearance in fractograph. At the A546, the semi-brittle fractograph appeared as shown in Fig. 6(d). From the above results, we can conclude that ductile dimple is related to the precipitation of η phase, and semi-brittle fractograph is related to the precipitation of η' phase and GP zones.

Conclusions

The decay of strength in weld HAZ was due to the precipitation and coarsening of η phase. In weld HAZ, the region of peak temperature 377 °C where containing the most precipitate of η phase had the lowest strength. The elongation was opposite to the precipitation of GP zones and η' phase, and was related to the precipitation of η phase in weld HAZ.

References

1. T. H. Sanders, Jr. and E. A. Starke, Jr., Metall. Trans. 7A, 1407 (1976).
2. B. Cina and B. Ranish, in Aluminum Industrial Products, Pittsburgh Chapter, Pittsburgh, American Society for Metals, Metals Park, OH (1974).

3. T. Kuroda, S. Kanamitsu, and T. Enjo, Transactions of JWRI. 19, 1, 87 (1990).
4. C. B. Sonnino, T. Ford, and V. Vanark, ASTM STP. 1134, 132 (1992).
5. Ranninger, British Corrosion Journal. 28, 2, 137 (1993).
6. J. M. Papazian, Metall. Trans. 12A, 269 (1981).
7. J. M. Papazian, Metall. Trans. 13A, 761 (1982).
8. C. W. Bartges, Scripta Metallurgica. 28, 1039 (1993).
9. D. J. Lloyd and M. C. Chaturvedi, J. Mater. Sci. 17, 1819 (1982).
10. J. K. Park and A. J. Ardell, Metall. Trans. 14A, 1843 (1983).
11. J. K. Park and A. J. Ardell, Mater. Sci. Eng. A114, 197 (1989).
12. J. K. Park and A. J. Ardell, Scripta Metallurgia. 1115 (1988).
13. M. Talianker and B. Cina, Metall. Trans. 20A, 2087 (1989).
14. F. Habiby, A. Ulhaq, F. H. Hashmi, and A. Q. Khan, Metall. Trans. 18A, 350 (1987).
15. J. K. Park and A. J. Ardell, Metall. Trans. 15A, 1531 (1984).
16. J. M. Papazian, Materials Science and Engineering. 79, 97 (1986).